Climate Dynamics (2003) 21: 659–675
DOI 10.1007/s00382-003-0343-3

G. A. Meehl · J. M. Arblaster

Mechanisms for projected future changes in south Asian monsoon precipitation

Received: 8 July 2002 / Accepted: 29 April 2003 / Published online: 4 November 2003

Abstract Results are first presented from an analysis of a global coupled climate model regarding changes in future mean and variability of south Asian monsoon precipitation due to increased atmospheric CO_2 for doubled ($2 \times CO_2$) and quadrupled ($4 \times CO_2$) present-day amounts. Results from the coupled model show that, in agreement with previous studies, mean area-averaged south Asian monsoon precipitation increases with greater CO_2 concentrations, as does the interannual variability. Mechanisms producing these changes are then examined in a series of AMIP2-style sensitivity experiments using the atmospheric model (taken from the coupled model) run with specified SSTs. Three sets of ensemble experiments are run with SST anomalies superimposed on the AMIP2 SSTs from 1979–97: (1) anomalously warm Indian Ocean SSTs, (2) anomalously warm Pacific Ocean SSTs, and (3) anomalously warm Indian and Pacific Ocean SSTs. Results from these experiments show that the greater mean monsoon precipitation is due to increased moisture source from the warmer Indian Ocean. Increased south Asian monsoon interannual variability is primarily due to warmer Pacific Ocean SSTs with enhanced evaporation variability, with the warmer Indian Ocean SSTs a contributing but secondary factor. That is, for a given interannual tropical Pacific SST fluctuation with warmer mean SSTs in the future climate, there is enhanced evaporation and precipitation variability that is communicated via the Walker Circulation in the atmosphere to the south Asian monsoon to increase interannual precipitation variability there. This enhanced monsoon variability occurs even with no change in interannual SST variability in the tropical Pacific.

G. A. Meehl (✉) · J. M. Arblaster
National Center for Atmospheric Research, Boulder, CO 80307-3000, USA
E-mail: meehl@ncar.ucar.edu

1 Introduction

Several previous modeling studies with increased CO_2 have shown that mean south Asian monsoon precipitation is likely to increase, with an accompanying enhancement of monsoon interannual variability (Meehl and Washington 1993; Kitoh et al. 1997; Hu et al. 2000; Lal et al. 2000, 2001; Douville et al. 2000; Cubasch et al. 2001; May 2002). The reasons for the increase in mean precipitation have been ascribed to warmer Indian Ocean SSTs in the future climate being able to supply an enhanced moisture source to fuel stronger monsoon rainfall as well as an intensified meridional temperature gradient over Asia as land areas warm faster than ocean (Kitoh et al. 1997; Douville et al. 2000; Lal et al. 2000).

Reasons for increased interannual variability have been more ambiguous. Meehl and Washington (1993) postulated that the warmer base state SSTs in the future climate would produce enhanced variability of evaporation over the Indian Ocean which would, in turn, then be transformed into greater variability of monsoon precipitation. This is illustrated in Fig. 1. The Clausius-Clapeyron relationship stipulates that saturation vapor pressure, e_s, is proportional to surface temperature squared (T^2). Thus, plotting this relationship in Fig. 1, for a given variation of surface temperature around the present-day mean climate (T_1), e_s has a given range of response. For the same variation of surface temperature in a future warmer climate (T_2), the range of response of e_s is greater. The implication is that this greater variability of e_s would provide greater variability of monsoon moisture source, and consequently greater variability of monsoon precipitation. However, one also could visualize this same type of process taking place over the tropical Pacific. There are

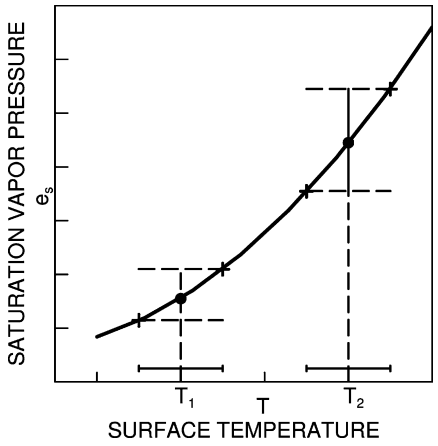

Fig. 1 Schematic diagram showing relationship between saturation vapor pressure, e_s, and surface temperature, T

well-known remote effects of tropical Pacific SSTs on the south Asian monsoon via the large-scale east-west circulation in the atmosphere associated with the Walker Circulation in observations (e.g. Rasmusson and Carpenter 1983; Meehl 1987; Webster and Yang 1992) and in model sensitivity experiments (e.g. Ju and Slingo 1995; Lau and Nath 2001; Slingo and Annamalai 2000; Meehl and Arblaster 2002), with warmer tropical Pacific SSTs generally associated with reduced monsoon rainfall. Thus, such remote effects could influence monsoon variability as well. Additionally, modeling studies have shown the effects of Indian Ocean SSTs on monsoon precipitation (e.g., Chandrasekar and Kitoh 1998; Meehl and Arblaster 2002).

The purpose of this study is to first analyze a current global coupled model to determine if, as seen in previous studies, the south Asian monsoon mean and variability become greater with increased CO_2 in CO_2 stabilization runs with doubled and quadrupled amounts of present-day CO_2. Then we will hypothesize reasons for these changes, and these hypotheses will be tested in a series of sensitivity experiments with the atmospheric model (from the coupled model) run with specified AMIP2 SSTs but with superimposed positive SST anomalies in the tropical Indian and Pacific Oceans.

In Sect. 2 we review the models and experiments used in this study, and in Sect. 3 we quantify the south Asian mean and interannual variability characteristics in the global coupled model, and pose hypotheses for why these characteristics should change with increasing CO_2. Then in Sect. 4 we describe results from the atmospheric model sensitivity experiments with anomalous SSTs in the tropical Indian and Pacific Oceans. A discussion and summary of the results and their implications are presented in Sect. 5.

2 Models and experiments

The Parallel Climate Model (PCM) is a fully coupled global ocean–atmosphere–sea ice-land surface model without flux adjustments (Washington et al. 2000; Meehl et al. 2001). It includes the CCM3 for the atmospheric component at T42 resolution (an equivalent grid spacing of roughly 2.8 by 2.8°) and 18 levels (hybrid coordinates; see details and references in Kiehl et al. 1998). The land surface component, the LSM, has specified vegetation types and a comprehensive treatment of surface processes (see Bonan 1998).

The PCM ocean component is a version of the Parallel Ocean Processor (POP) with 32 levels in the vertical and 2/3° nominal latitude-longitude resolution reduced to 0.5° in latitude in the tropics (actual longitudinal grid spacing in the equatorial Pacific ranges from about 0.6° in the east to 0.9° in the west due to the effects of the rotated pole over northern North America). The PCM ocean component uses biharmonic diffusion horizontal mixing and Pacanowski-Philander vertical mixing. The PCM sea-ice scheme has thermodynamic and dynamic components (Washington et al. 2000).

Results from a 300 year period in the control run with the PCM are analyzed here. Additionally, CO_2 is increased at 1% per year compound in the model and stabilized at doubling and quadrupling (with respect to present-day values) for about 150 years each. Only CO_2 concentration is changed in these experiments. The last 100 years of these stabilization (i.e., CO_2 concentration held constant at $2 \times CO_2$ and $4 \times CO_2$) experiments are analyzed here. Though the mean climate is slowly changing (about 0.05 °C per decade for $2 \times CO_2$ and roughly 0.10 °C per decade for $4 \times CO_2$) over these time periods (Washington et al. 2000), the changes are relatively small with the forcing held fixed compared to a transient experiment where the forcing is rapidly changing. The former allows a more stable climate in which to assess changes in monsoon features. The stabilization results from the PCM are also more directly comparable to the sensitivity experiments with specified SSTs.

The sensitivity experiments use a version of the atmospheric model (CCM3 at T42 18L) in the PCM. Observed sea surface temperatures (SSTs) are specified and time varying from 1979–1997. Details of these experiments are described in Sect. 4.

3 Global coupled model results

Mean June–July–August rainfall for the Indo-Pacific region from the PCM is shown for the 300 year control run (Fig. 2a), as well as precipitation differences for the last 100 years of the stabilized $2 \times CO_2$ (Fig. 2b) and $4 \times CO_2$ (Fig. 2c) integrations minus the 300 year control run. Stippling in Fig. 2b, c indicates local significance at the 10% level from a student t test. The climatological pattern of precipitation in the coupled model control run (Fig. 2a) is similar to a global coupled model with the same atmosphere but different ocean, the Climate System Model (CSM, Meehl and Arblaster 1998), and also similar to the pattern produced by the atmosphere run with observed SSTs (Meehl and Arblaster 1998, 2002). The precipitation maxima south of India and over eastern India, Bangladesh and Bay of Bengal are well-simulated compared to observations. There is somewhat deficient precipitation over northwestern India and west of the Indian peninsula, with overestimated precipitation over the Himalayas. An area-averaged seasonal monsoon precipitation index (JJA rainfall averaged over all grid points in the area 5°N–40°N, 60°E–100°E) is 4.7 mm day^{-1} (the observed value for the same time period from the Xie and Arkin (1996) precipitation dataset is 5.3 mm day^{-1}). This area is larger than the all-India monsoon rainfall index of Parthasarathy et al. (1991) that includes rainfall only over the country of

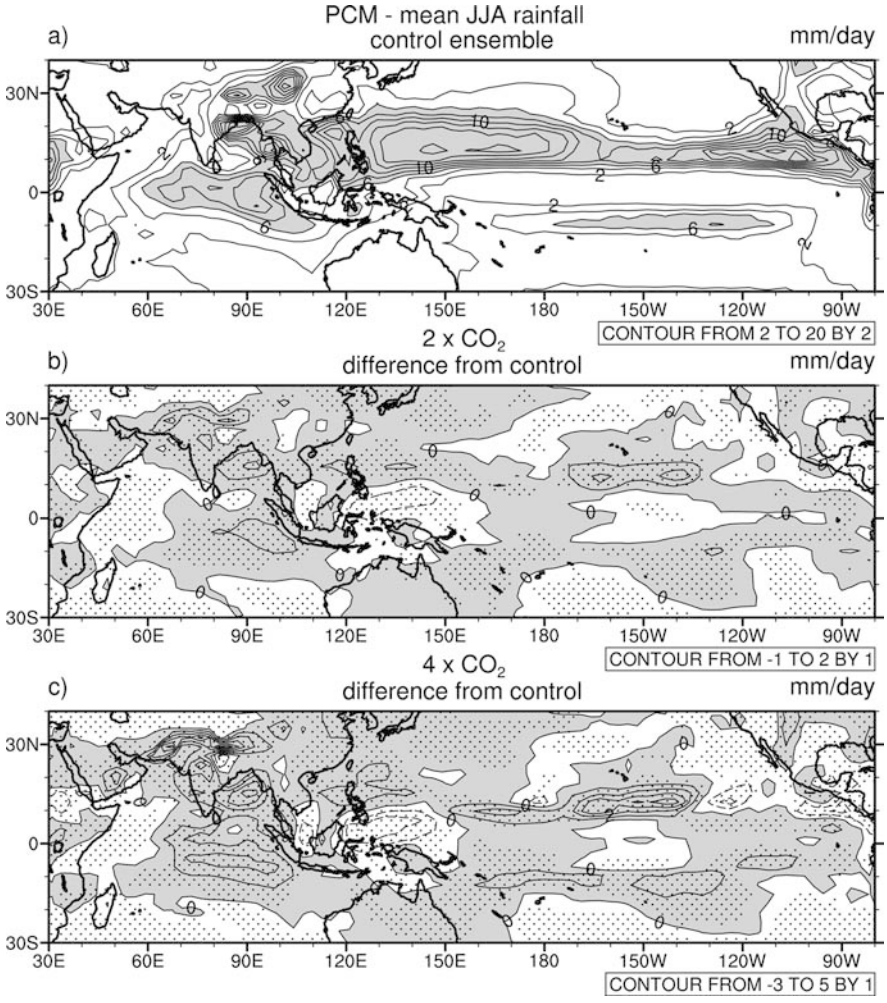

Fig. 2 **a** JJA season mean rainfall averaged over a 300 year period in the control run of the PCM (coupled model), contour interval 2 mm day^{-1}, *values* greater than 6 mm day^{-1} *shaded*; **b** 100 year stabilized 2 × CO_2 experiment minus control precipitation, JJA, contour interval 1 mm day^{-1}, *positive areas shaded*, *stippling* indicates areas exceeding 10% significance level from a student *t* test of the differences; **c** same as **b** except for 4 × CO_2

India. There is evidence of a double ITCZ in the tropical Pacific typical of this class of model run without flux adjustment (Meehl et al. 2001).

Figure 2b shows the difference, 2 × CO_2 minus control, for precipitation over this same region. There are statistically significant positive precipitation differences of over 1 mm day^{-1} over many areas of India, as well as increases over the tropical Indian Ocean and the ITCZ areas of the Pacific. The area-averaged monsoon precipitation index is 5.1 mm day^{-1}, or an increase of about 9% compared to the control run. For 4 × CO_2 minus control (Fig. 2c), the pattern is essentially the same as for 2 × CO_2 except the magnitude of the differences is greater, in some areas more than doubled (e.g., equatorial Indian Ocean, northern India, Pacific ITCZ and SPCZ) indicating local areas of non-linear response. The area-averaged monsoon precipitation index increases to 5.6 mm day^{-1}, an increase from the control of 19%, and greater than the 2 × CO_2 case by 10%.

Interannual standard deviations of JJA rainfall from the PCM for the control run are shown in Fig. 3a. In general, maximum values of standard deviation coincide with maximum values of precipitation in Fig. 2a over the equatorial Indian Ocean and ITCZ region in the Pacific. Additionally, there are large values over 2 mm day^{-1} in Fig. 3a in northern and central India and Pakistan in the marginal precipitation zones in Fig. 2a. The interannual standard deviation of area-averaged rainfall for the Indian monsoon index is 0.37 mm day^{-1}, with the observed value from the Xie and Arkin (1996) observations of 0.39 mm day^{-1}. The somewhat less than observed value for the PCM for the Indian monsoon region is reflected in the Pacific sector as well. Area averaged standard deviation for 20°N–20°S, 150°E–150°W, for the PCM is 1.58 mm day^{-1}, while for observations the value is 1.64 mm day^{-1}. This is likely related to the colder-than-observed base state SSTs in the tropical oceans in the PCM of 1–2 °C (Washington et al. 2000; Meehl et al. 2001), and the relationship to evaporation variability discussed later.

Figure 3b, c shows differences of JJA rainfall standard deviations for 2 × CO_2 minus control and 4 × CO_2 minus control, respectively, with stippling indicating the 10% significance level from an f test on the ratio of the variances. There are increases of precipitation variability over much of the Indian monsoon region for both 2 × CO_2 and 4 × CO_2. Increased variability of rainfall is

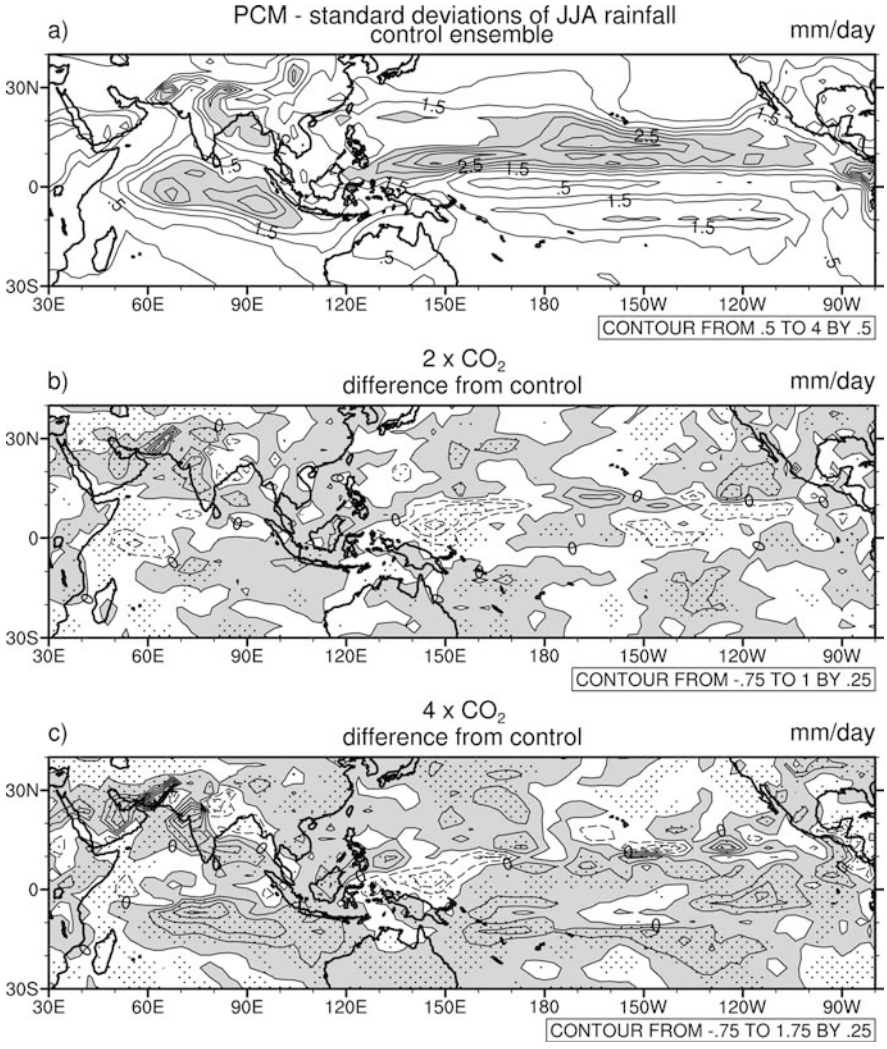

Fig. 3 **a** JJA interannual standard deviation of rainfall for 300 year period in the control run of the PCM (coupled model), contour interval 0.5 mm day^{-1}, *values* greater than 2 mm day^{-1}*shaded*; **b** 100 year stabilized $2 \times CO_2$ PCM experiment minus control standard deviation of precipitation, JJA, contour interval 0.25 mm day^{-1}, *positive areas shaded*, *stippling* indicates areas exceeding 10% significance level from an *f* test on the ratio of the variances; **c** same as **b** except for $4 \times CO_2$

particularly significant for $4 \times CO_2$ over the tropical south Indian Ocean (differences greater than $+0.8$ mm day^{-1}) and over the central equatorial Pacific Ocean with values greater than $+0.5$ mm day^{-1}. The standard deviation of area-averaged rainfall for the Indian monsoon index for the $2 \times CO_2$ experiment is 0.47 mm day^{-1}, and is similar for $4 \times CO_2$ at 0.46 mm day^{-1}. These represent increases of about 27% from the control. Since both positive and negative differences increase, the area-averaged monsoon precipitation index is about the same for $2 \times CO_2$ and $4 \times CO_2$.

In any case, the results from Figs. 2 and 3 indicate that, for increased CO_2, the PCM shows an increase of mean Indian monsoon rainfall and increased monsoon interannual variability in agreement with studies cited previously. The question we will now address is why do these changes in Indian monsoon precipitation occur? Timmermann et al. (1999) showed an increase of interannual variability of tropical pacific SSTs in a warmer future climate. Hu et al. (2000) showed this contributes to enhanced south Asian monsoon variability. However, Washington et al. (2000) note that the interannual variability of tropical Pacific SSTs does not significantly change with increased CO_2 in the global coupled model analyzed in the present work (the PCM).

Following earlier studies (e.g., Meehl and Washington 1993; Kitoh et al. 1997; Douville et al. 2000), we propose that the increased mean precipitation can arise from increased Indian Ocean SST which produces an enhanced moisture source for monsoon rainfall. Concerning the increase of interannual variability, following Fig. 1 we hypothesize that (1) the warmer Indian Ocean SSTs with increased CO_2 produce a non-linear enhancement of the moisture source variability that translates into increased monsoon rainfall variability, and (2) a similar process occurs in the tropical Pacific that affects monsoon variability through the large-scale east-west (Walker) circulation in the atmosphere.

Washington et al. (2000) show surface temperature increases over south Asia for $2 \times CO_2$ of about 2 °C, while SSTs over the Indian Ocean increase about 1 °C. For $4 \times CO_2$ the increases over land are greater than 4 °C, while over the Indian Ocean the warming is about 2.5 °C. Therefore, it could be possible that the enhanced meridional temperature gradient could be

contributing to increased monsoon rainfall with increased CO_2 as well as the associated increased moisture source from the warmer Indian Ocean. Similarly, the warmer SSTs in the tropical Indian and Pacific Oceans could produce greater evaporation variability and thus contribute to enhanced moisture source and monsoon rainfall variability. However, in a separate modeling study Meehl and Arblaster (2002) show that the SST forcing is greater than meridional temperature gradients for interannual variability of monsoon rainfall. Consequently, the SST-related aspects of monsoon rainfall in a warmer climate, both in terms of changes in mean and interannual variability, will be addressed here.

4 GCM sensitivity experiments

To test these hypotheses we will analyze results from a series of three sensitivity experiments with the atmospheric model taken from the PCM and run with AMIP2 SSTs (for description see http://www-pcmdi.llnl.gov/amip/AMIP2EXPDSN/BCS/bcsintro.html), but with SST anomalies superimposed in the Indian and Pacific oceans. The areas where the SSTs are increased are shown in Fig. 4. We first add a uniform increase to the AMIP2 SSTs over the Indian Ocean of +1 °C for an ensemble of three experiments (1979–97). Next we add an increase of +1.25 °C over the Pacific for another ensemble of three experiments. Finally, we combine the SST increases over the Indian and Pacific oceans and run an ensemble of three experiments. The locations and magnitudes of these SST increases are derived from the difference plots for surface temperature for a doubling of CO_2 in the PCM as noted already (Washington et al. 2000). The results from the model experiments are compared to two control runs with the AMIP2 SSTs without any SST anomalies added. In all the sensitivity experiments, the CO_2 concentrations remain at the present-day value. Therefore, the atmosphere is warmer in the coupled model CO_2 experiment due to radiative effects of increased CO_2 and associated feedbacks. In the sensitivity experiments we can only examine the model response to changes in SST. Additionally, the interannual variations of the SSTs are the same in all sensitivity experiments. Thus, differences in rainfall variability are due to changes in base state SSTs.

4.1 Mean rainfall

Mean JJA rainfall averaged for the two control experiments is shown in Fig. 5a. As documented earlier for the CCM3 (e.g., Meehl and Arblaster 1998), the rainfall distribution over the Indian monsoon region is better simulated than for the PCM in Fig. 2a, though both represent many of the salient features of monsoon rainfall including the maximum over the equatorial Indian Ocean, and the maximum over the Bay of Bengal extending across India comparable to other models of this class (e.g., Douville et al. 2000). The area-averaged monsoon rainfall index for the CCM3 control runs is 6.9 mm day^{-1}, compared to the observed value for the 1979–1997 period mentioned earlier of 5.3 mm day^{-1}.

For the warm Indian Ocean sensitivity experiments, the ensemble average minus the mean of the two control runs is shown in Fig. 5b. There are statistically significant increases of precipitation not only over the Indian Ocean (greater than 3 mm day^{-1}), but also over much of India itself. This is consistent with other similar sensitivity experiments with the CCM3 and warm Indian Ocean SSTs (Meehl and Arblaster 2002). They showed this increase was due to intensified evaporation from the warmer water which not only increases precipitation over the ocean but also contributes to an enhanced moisture source for greater precipitation over India (also shown by May 2002). This is also the case here. The area-averaged JJA monsoon rainfall index for the warm Indian Ocean experiments is 8.2 mm day^{-1}, an increase over the control of about 19%. Due to the connections via the Walker Circulation, there are statistically significant decreases of 2–3 mm day^{-1} in the far western Pacific and SPCZ regions.

It is worth noting that increased monsoon precipitation in model experiments generally occurs if the entire tropical Indian Ocean is anomalously warm (see Meehl and Arblaster 2002). If only the equatorial Indian Ocean is anomalously warm (as in Chandrasekar and Kitoh 1998), there is an anomalous increase of precipitation only over the warmer water south of India and suppressed precipitation over India itself.

Figure 5c shows the ensemble average minus the mean of the two control runs for the warm Pacific sensitivity experiments. There are statistically significant increases of precipitation over the region in the tropical Pacific where the SSTs are increased of around 10 mm day^{-1}, partly due to a southward shift of the

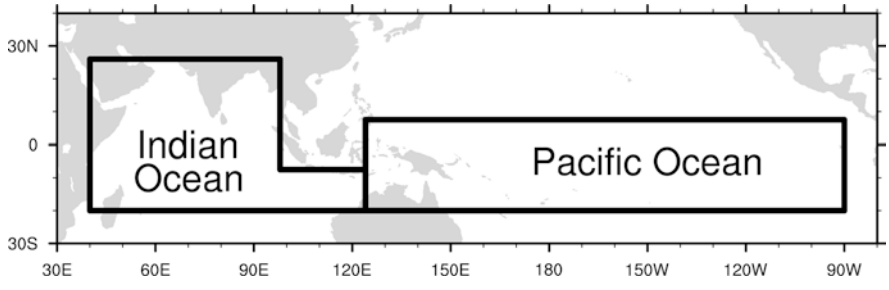

Fig. 4 SSTs for ocean points within the boxes are increased in the AMIP2-type sensitivity experiments. Indian Ocean SST increases are 1.0 °C, and Pacific Ocean SST increases are 1.25 °C

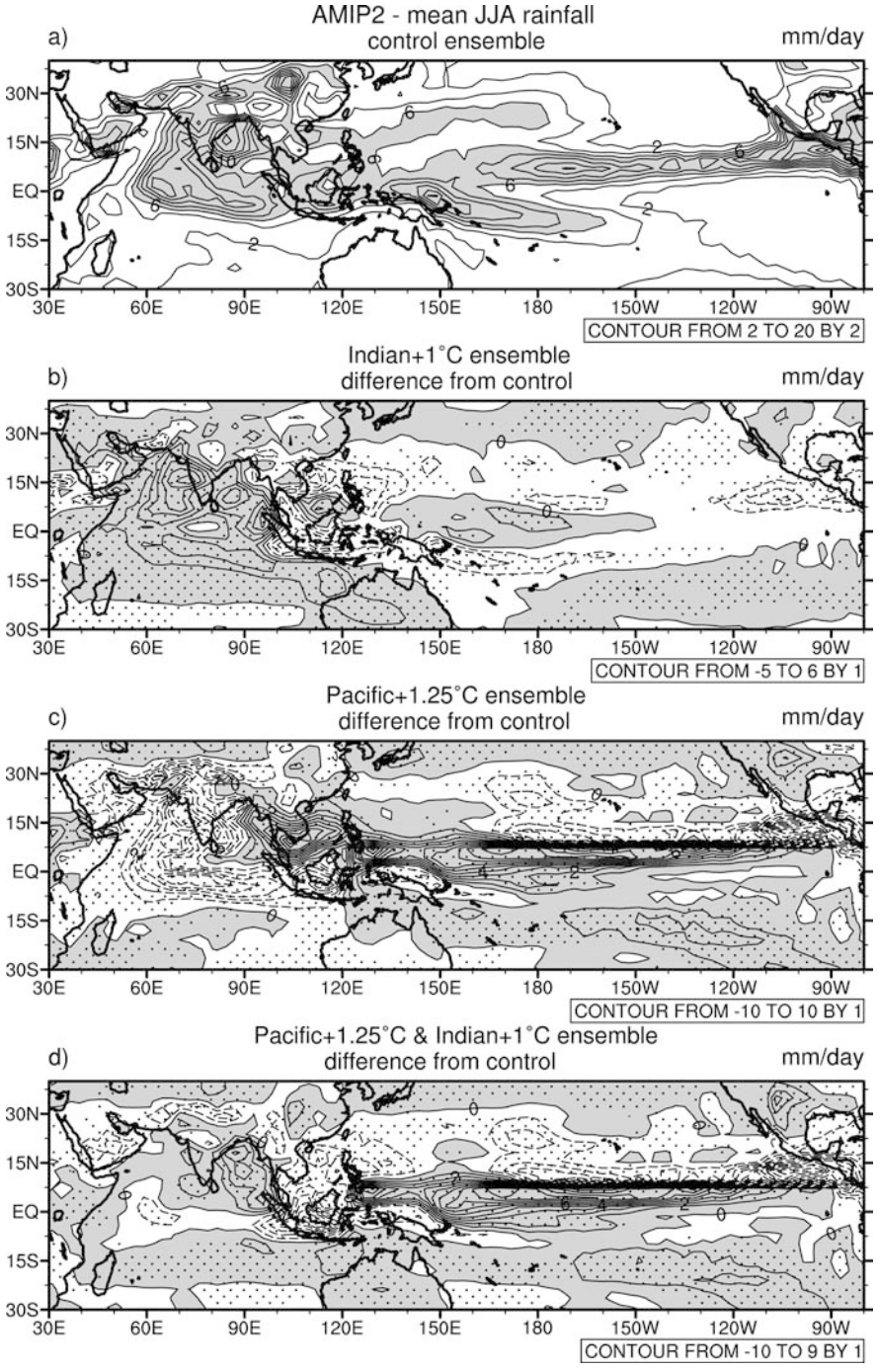

Fig. 5 **a** JJA mean rainfall averaged over two control runs with AMIP2 SSTs, 1979–97, specified in the atmospheric model, contour interval 2 mm day^{-1}, *values* greater than 6 mm day^{-1} *shaded*; **b** three member ensemble average for the warm Indian Ocean SST experiment (Indian Ocean points outlined in Fig. 4 increased by 1 °C) minus control precipitation, JJA, contour interval 1 mm day^{-1}, *positive areas shaded*, *stippling* indicates areas exceeding 10% significance level from a student *t* test on the differences; **c** same as **b** except for the warm Pacific case (Pacific Ocean points outlined in Fig. 4 increased by 1.25 °C); **d** same as **b** except for the warm Indian/warm Pacific case

ITCZ and a northward movement of the SPCZ. As could be expected from the connections via the large-scale east-west circulation in the atmosphere (e.g., Meehl 1987) noted in Fig. 5b, these increases are accompanied by statistically significant decreases over the Indian sector of about 8 mm day^{-1}. Consequently, the area-averaged JJA monsoon rainfall index for the warm tropical Pacific Ocean experiments is 5.8 mm day^{-1}, a decrease from the control of roughly 16%.

The ensemble mean differences for experiment with both the Indian Ocean and Pacific Ocean anomalously warm (minus the control run average) are shown in Fig. 5d. There are statistically significant increases of precipitation in the ITCZ region in the Pacific with values greater than 9 mm day^{-1}. The increases seen in Fig. 5b over the Indian sector are now reduced with statistically significant maxima in the Bay of Bengal exceeding 3 mm day^{-1}, with many areas of precipitation change over India itself not statistically significant. The area-averaged monsoon rainfall index for the warm Indian and Pacific Ocean runs is 7.3 mm day^{-1}, decreased 11% from 8.2 mm day^{-1} in Fig. 5b for just the warm Indian Ocean, but increased 26% from the warm Pacific Ocean value of 5.8 mm day^{-1}. Though the combined

value of 7.3 mm day^{-1} is in between the warm Indian Ocean and warm Pacific Ocean values, it is still greater than the control run value of 6.9 mm day^{-1} by 6%.

Therefore, the effect of the anomalously warm Indian Ocean by itself is to increase monsoon precipitation by 19%, but warming the Pacific by itself reduces monsoon precipitation by 16%. With both the tropical Indian and Pacific Oceans anomalously warmer, monsoon precipitation only increases by 6%. Later we will document this in relation to changes in the large-scale east-west circulation as indicated by omega (vertical velocity). Those results will show the tendency for suppression of monsoon rainfall from processes in the tropical Pacific competing with the tendency for increase of monsoon rainfall from the increased Indian Ocean SSTs as noted in Fig. 5. In any case, for the analogue to an increase of CO_2 where both Indian and Pacific Oceans warm, there is still an increase of area-averaged monsoon precipitation that is comparable to that seen for a doubling of CO_2 from the PCM of 9%, though there are local differences in the patterns of the changes. However, the land temperatures are free to change in unspecified ways in the CCM3 sensitivity experiments. Without any enhancement of meridional temperature gradient, just an increase of Indian Ocean SSTs (combined with an increase of Pacific Ocean SSTs), can cause a modest increase of mean monsoon rainfall comparable to that seen in the coupled model for a doubling of CO_2. Therefore, we conclude that most of the mean monsoon precipitation increase can be caused by increased ocean temperatures alone, with enhanced meridional temperature gradient effects a secondary forcing. This is consistent with the results of Kitoh et al. (1997) and May (2002) for increased CO_2, and also goes along with the model results of Meehl and Arblaster (2002) who showed a similar result in a different context.

4.2 Interannual variability

Of interest here are the reasons for the enhanced interannual variability of monsoon precipitation with increased CO_2 seen in the coupled model. Interannual standard deviations of JJA rainfall are shown in Fig. 6 from the AMIP2-type sensitivity experiments. Similar to the coupled model, the greatest values of interannual JJA standard deviation in Fig. 6a for the concatenated control runs tend to coincide with JJA season mean precipitation maxima in Fig. 5a over the equatorial Indian Ocean, Bay of Bengal, and the ITCZ region in the Pacific, and in the marginal precipitation zones of western and northwestern India. The JJA area-averaged monsoon standard deviation for the control run is 0.49 mm day^{-1}, with the observed value from the Xie and Arkin (1996) data of 0.39 mm day^{-1}. This somewhat greater than observed value of area-averaged standard deviation over the Indian monsoon region is also seen in the Pacific sector in Fig. 6a. For 20°N–20°S, 150°E–150°W, the area-averaged standard deviation from the model is 2.01 mm day^{-1}, compared to the observed value of 1.64 mm day^{-1}.

Figure 6b shows the difference of interannual standard deviations calculated for the warm Indian Ocean concatenated ensemble minus control values in Fig. 6a, with stippling indicating the 10% significance level from an *f* test on the ratio of the variances. Rainfall variability increases over parts of eastern India and the Bay of Bengal, but there are decreases over northwestern India. The area-averaged monsoon standard deviation for the warm Indian Ocean experiments is 0.47 mm day^{-1}, a slight decrease compared to the control run of 0.49 mm day^{-1}. Therefore, the enhanced moisture variability in the Indian Ocean alone from the mechanism in Fig. 1 does not seem to consistently increase interannual variability of precipitation over the Indian monsoon region in the CCM3 sensitivity experiments. It is interesting to note that there are increases of precipitation variability in the equatorial western and Central Pacific of up to 1 mm day^{-1} suggesting that some of the enhanced regional variability in the Indian Ocean is being communicated to the Pacific by the Walker Circulation.

For the warm Pacific Ocean experiments in Fig. 6c, there are significant increases of precipitation variability where the water is anomalously warm, with differences of up to +2 mm day^{-1}. Interestingly, as was seen in Fig. 6b for the warm Indian Ocean experiments, there is enhanced precipitation variability to the west over southeast Asia and the near-equatorial Indian Ocean with values in these regions exceeding 2 mm day^{-1}. As in Fig. 6b, this implies enhanced precipitation variability is being communicated from the Pacific to the Indian sector by the Walker Circulation. In fact, the increases over northern and eastern India and those over the Indian Ocean just south of India contribute to an interannual area-averaged monsoon standard deviation of 0.62 mm day^{-1}, an increase over the control run of 27%.

In Fig. 6d for the warm Indian Ocean plus warm Pacific Ocean, the area-averaged monsoon standard deviation is 0.57 mm day^{-1}, an increase of 16% over the control. This can be compared to an increase for doubled CO_2 in Fig. 3b of 27%. The geographic plot of the standard deviation differences in Fig. 6d shows significantly enhanced precipitation variability over much of India, the Bay of Bengal and the tropical Indian Ocean. Additionally, over the Pacific there are large significant increases of precipitation variability with maximum standard deviation differences greater than +2.0 mm day^{-1}. Therefore, the enhancement of area-averaged monsoon variability in the sensitivity experiments appears to emanate mainly from the tropical Pacific in these experiments.

4.3 Moisture source processes

To look in greater detail at the moisture source process and to address the hypotheses posed earlier, standard deviations of concatenated JJA latent heat flux

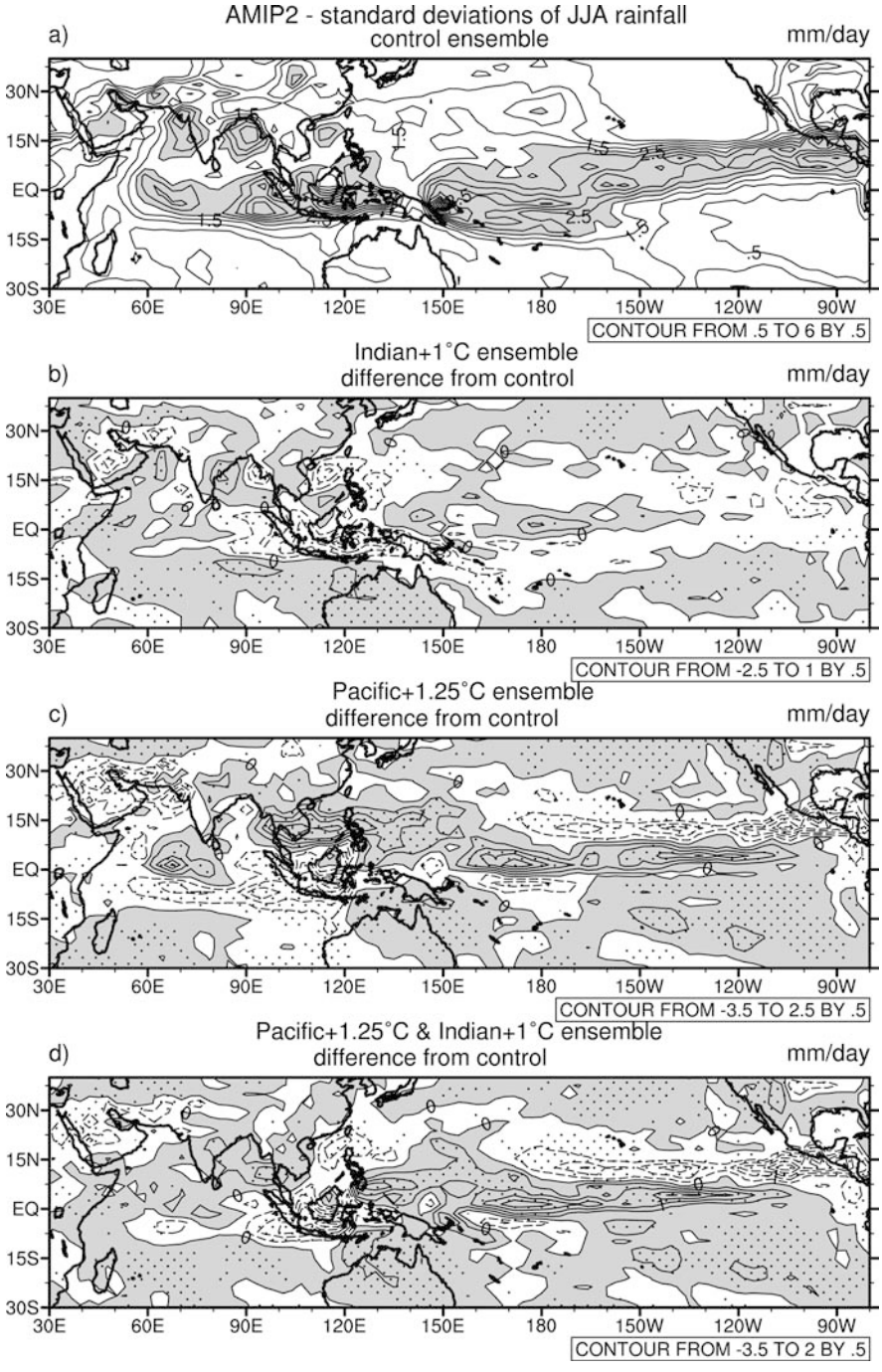

Fig. 6 **a** JJA interannual precipitation standard deviations calculated for the two concatenated control runs with AMIP2 SSTs, 1979–97, contour interval 0.5 mm day^{-1}, *values* greater than 2 mm day^{-1} *shaded*; **b** concatenated three member ensemble interannual rainfall standard deviations for the warm Indian Ocean SST experiment minus control precipitation standard deviations, JJA, contour interval 0.5 mm day^{-1}, positive areas shaded, stippling indicates areas exceeding 10% significance level from an *f* test on the ratio of the variances; **c** same as **b** except for the warm Pacific case; **d** same as **b** except for the warm Indian/warm Pacific case

(indicative of evaporation variability) from the AMIP2-type experiments are shown for the control (Fig. 7a), and standard deviation differences (stippled areas indicate 10% significance for an *f* test on the ratio of the variances) for the warm Indian Ocean (Fig. 7b), the warm Pacific Ocean (Fig. 7c), and warm Indian/warm Pacific Ocean (Fig. 7d) experiments. Largest standard deviations for the control (Fig. 7a) generally lie over the tropical oceans with values greater than 20 W m^{-2}. For the warm Indian Ocean minus control in Fig. 7b, there is significantly increased latent heat flux variability of around 5 W m^{-2} over most of the southern Arabian Sea and western Indian Ocean, but decreased variability over the Bay of Bengal. For the warm Pacific Ocean experiments in Fig. 7c, there is significantly enhanced latent heat flux variability of over 15 W m^{-2} in the equatorial western Pacific and ITCZ, extending across southeast Asia to the Indian Ocean and India itself, with differences in those locations roughly +5 to +10 W m^{-2}. The warm Indian/warm Pacific Ocean experiments in Fig. 7d also show a significant enhancement of latent heat flux variability over the western tropical Pacific, southern Bay of Bengal, and India itself with differences around 5 to 10 W m^{-2}. Area-averaged standard deviation of latent

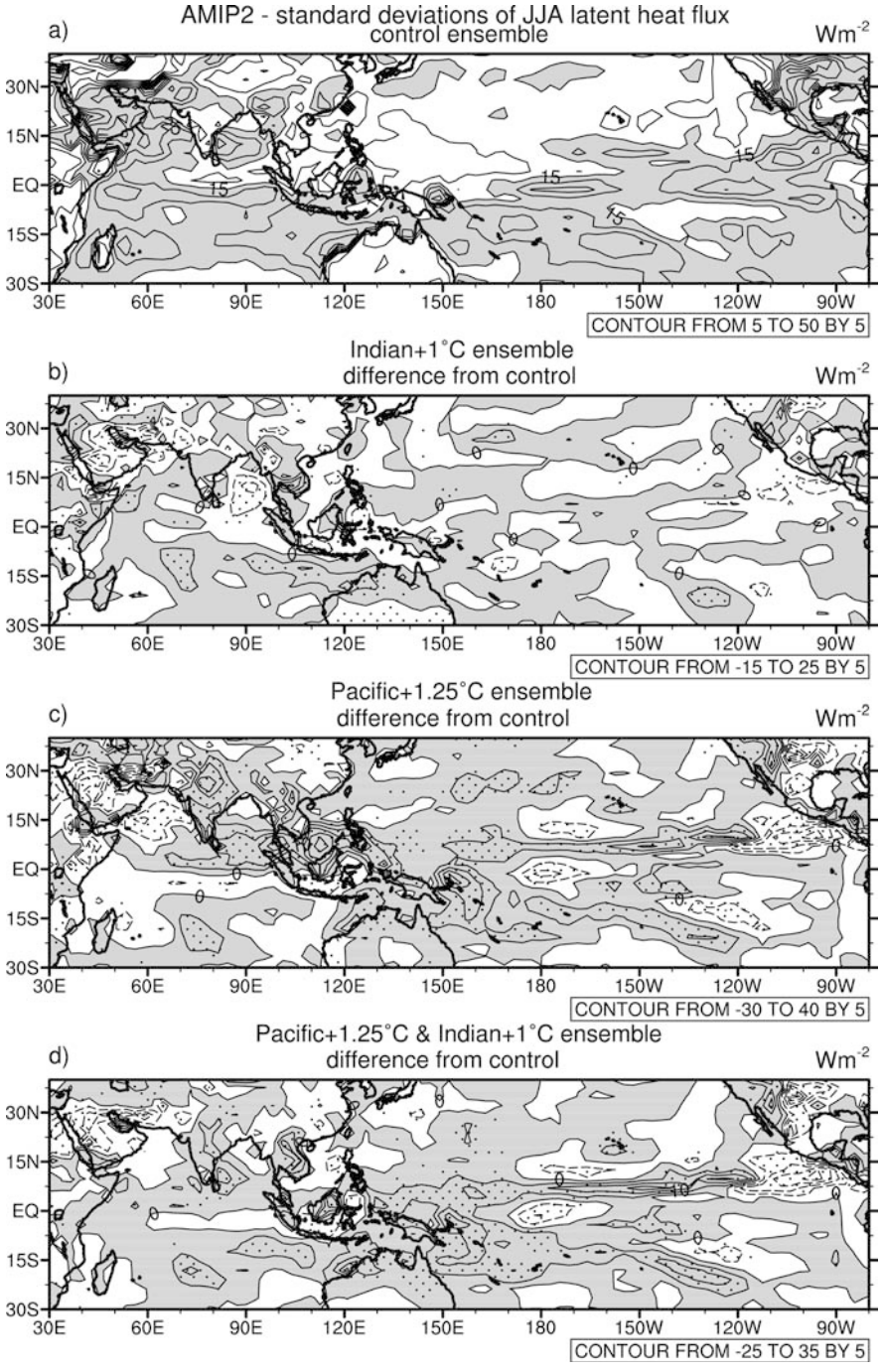

Fig. 7 **a** JJA interannual latent heat flux standard deviations calculated for the two concatenated control runs with AMIP2 SSTs, 1979–97, contour interval 5 W m^{-2}, *values* greater than 15 W m^{-2}*shaded*; **b** concatenated three member ensemble interannual latent heat flux standard deviations for the warm Indian Ocean SST experiment minus control latent heat flux standard deviations, JJA, contour interval 5 W m^{-2}, *positive areas shaded*, *stippling* indicates areas exceeding 10% significance level from an *f* test on the ratio of the variances; **c** same as **b** except for the warm Pacific case; **d** same as **b** except for the warm Indian/warm Pacific case

heat flux from the moisture source region in the tropical Indian Ocean (10°N–10°S, 50–95°E) for the control is 8.2 W m^{-2}, and for the warm Indian Ocean experiments is 8.9 W m^{-2}. However, for the warm Indian/warm Pacific Ocean this drops to 7.9 W m^{-2}.

Thus, though the mechanism for enhanced evaporation and hence latent heat flux variability in Fig. 1 seems to be working in some of the moisture source areas of the Indian Ocean for the warm Indian Ocean experiments in Fig. 7b (the southern Arabian Sea and western Indian Ocean), those increases do not translate to overall enhanced monsoon precipitation variability in Fig. 6b. Warming the Pacific not only increases latent heat flux variability over the areas where the water has been specified to be warmer, but also over large areas of the tropical Indian Ocean and India itself (Fig. 7c). Reasons for this are addressed in the next section. Meanwhile, the warm Indian/warm Pacific Ocean experiments actually decrease the latent heat flux variability over parts of India (e.g., positive differences in Fig. 7c over northern India of 15 W m^{-2} decrease to 5 W m^{-2} in Fig. 7d), while the contribution of the warmer Indian Ocean SSTs combined with warmer Pacific SSTs has less effect over the Indian Ocean itself (negative

differences in Fig. 7c over the Arabian Sea increase to near zero in Fig. 7d but there is still enhanced variability over most of the tropical Indian Ocean). The increases in latent heat flux variability are greater in the tropical western Pacific than the tropical Indian Ocean in general with anomalously warmer SSTs. This is consistent with the warmer base state SSTs in the western Pacific warm pool. Also recall that in the sensitivity experiments, the baseline SST variability does not change. These changes in latent heat flux variability in the tropical western Pacific are occurring in large part due to the mechanism outlined in Fig. 1.

4.4 Large-scale east-west (Walker) circulation

It was suggested earlier in Fig. 5 that changes to the large-scale east-west (Walker) atmospheric circulation could be influencing the monsoon precipitation such that the warmer Indian Ocean by itself would intensify the monsoon, but the combination of warm Indian Ocean and warm Pacific Ocean would produce less of an increase due to the competing effect of large-scale suppression of precipitation from the Pacific. To investigate this contention, Fig. 8a shows vertical velocity (omega) for the control ensemble averaged from 15°S to 25°N, thus accounting for most areas of tropical convection and precipitation in Fig. 5a, such as west of 120°E in the Indian Ocean, and in the Pacific east of 120°E, in particular the western Pacific west of 170°E. Negative values indicate upward motion. There are large negative values over the longitudes of the Indian monsoon (60°E to 90°E) with maxima in excess of 40 hPa $s^{-1} \times 10^{-5}$. There are lower amplitude maxima of upward vertical velocity over the western Pacific from 150°E to the dateline with values greater than 20 hPa $s^{-1} \times 10^{-5}$.

Figure 8b is a plot of the difference, warm Indian Ocean minus control, showing negative values of around –20 hPa $s^{-1} \times 10^{-5}$ over the Indian monsoon longitudes (anomalous upward motion associated with enhanced monsoon precipitation in Fig. 5b), with anomalous subsidence (positive values of roughly +10 hPa $s^{-1} \times 10^{-5}$) over the western Pacific. Differences in Fig. 8 with amplitudes greater than about 2 hPa $s^{-1} \times 10^{-5}$ are significant at the 10% level (not shown). Associated with these changes in vertical velocity, there are implied anomalous easterly winds from the western Pacific into the Indian Ocean in the lower troposphere, and the opposite in the upper troposphere. For the warm Pacific ensemble difference in Fig. 8c, negative anomalies of omega, indicating enhanced upward motion of over –10 hPa $s^{-1} \times 10^{-5}$, occur over the longitudes of the tropical Pacific associated with the increased precipitation there in Fig. 5c from around 120°E to 120°W. There is also anomalous subsidence (positive values with maxima greater than +30 hPa $s^{-1} \times 10^{-5}$) over the Indian Ocean longitudes from about 50°E to 90°E. Thus, the vertical motion anomalies have almost the opposite signs from those in Fig. 8b. The implied anomalous zonal winds are also opposite to those for the warm Indian Ocean case in Fig. 8b.

For the warm Indian/warm Pacific Ocean ensemble average difference in Fig. 8d, the combined influence of the positive Pacific and Indian Ocean SST anomalies is seen in terms of anomalous upward motion in both basins with values of over –10 hPa $s^{-1} \times 10^{-5}$ from 150°E to 120°W in the Pacific, in addition to anomalous upward motion near 90°E in the Indian monsoon region with values over –10 hPa $s^{-1} \times 10^{-5}$. Associated with these upward motion anomalies, there is anomalous downward motion of around +10 hPa $s^{-1} \times 10^{-5}$ near 50–60°E, and roughly +20 hPa $s^{-1} \times 10^{-5}$ from 100–120°E. The latter is interesting in the context of the separate ocean basin results in Figs. 8b, c. Anomalous upward motion in the Indian and Pacific Ocean regions (seen separately in Fig. 8b, c) produces upper level convergence near 110°E that is then associated with anomalous subsidence there in Fig. 8d.

Comparing Fig. 8b–d, the effect of the warm SSTs in the tropical Pacific is to enhance precipitation and anomalous vertical motion there, and cause anomalous subsidence in the Indian sector that competes with the effects of the warmer Indian Ocean SSTs that are producing anomalous precipitation and upward motion. The net effect in Fig. 8d of the warm tropical Pacific SSTs in combination with warm Indian Ocean SSTs is to dramatically reduce the anomalous upward vertical motion over the Indian sector seen in Fig. 8b when just the Indian Ocean SSTs are warm. This is due to the remote influence on the Indian sector of vertical motion in the Pacific transmitted by the large-scale east-west circulation (Walker Circulation) in the atmosphere.

One could imagine that similar effects from the Pacific are being transmitted via the anomalous east-west atmospheric circulation in terms of interannual variability as well. In Fig. 9 the interannual standard deviations of vertical motion (omega) are shown. For the control run (Fig. 9a) there are values of interannual variability of omega greater than 5 hPa $s^{-1} \times 10^{-5}$ at nearly all longitudes, indicative of both positive and negative vertical velocity variability. For the warm Indian Ocean minus control values in Fig. 9b, there is a mixture of positive and negative omega anomalies over the warm Indian Ocean sector consistent with the mixture of positive and negative precipitation standard deviations in Fig. 6b. There are also small increases in omega variability (values around 1 hPa $s^{-1} \times 10^{-5}$) associated with anomalous downward motion in Fig. 8b in the Pacific from about 130°E to 170°W. Differences in Fig. 9 greater than about 1 hPa $s^{-1} \times 10^{-5}$ are significant at the 10% level (not shown).

When just the tropical Pacific is anomalously warm (Fig. 9c), there is enhanced vertical velocity variability (values greater than 2 hPa $s^{-1} \times 10^{-5}$) spanning the western Pacific warm pool and extending to the Indian Ocean. In comparing Fig. 9c to Fig. 8c, it can be seen

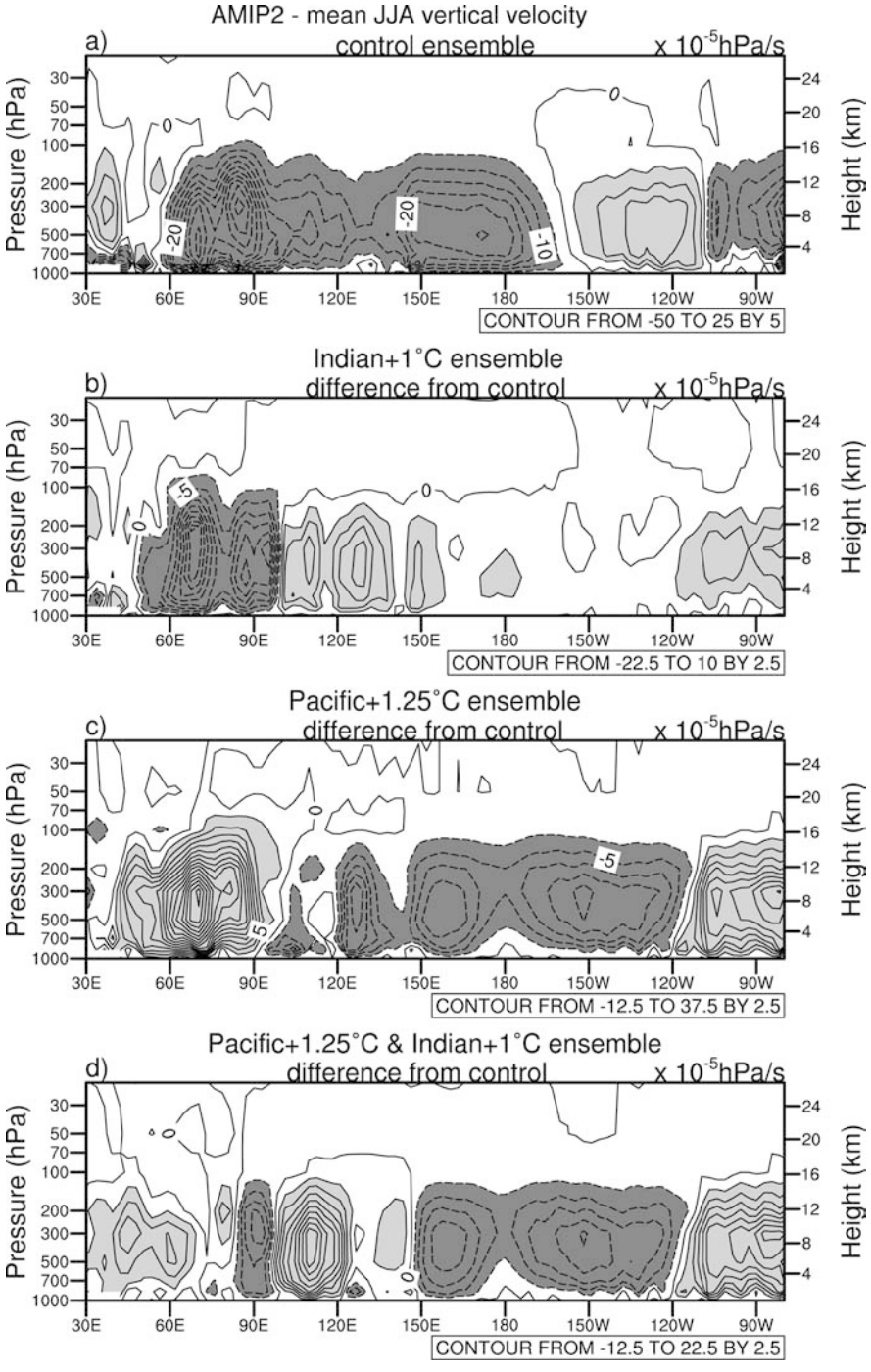

Fig. 8 **a** JJA mean omega (vertical velocity) averaged over two control runs with AMIP2 SSTs, 1979–97, specified in the atmospheric model, 10°S to 15°N, contour interval 5 hPa $s^{-1} \times 10^{-5}$, *values* greater than 5 hPa $s^{-1} \times 10^{-5}$*shaded*; **b** three member ensemble average for the warm Indian Ocean SST experiment minus control omega, JJA, contour interval 2.5 hPa $s^{-1} \times 10^{-5}$, *dashed negative values* (enhanced upward vertical velocity) exceeding –2.5 hPa $s^{-1} \times 10^{-5}$ are *dark shaded*, positive areas (enhanced downward vertical velocity) greater than +2.5 hPa $s^{-1} \times 10^{-5}$ are *light shaded*, **c** same as **b** except for the warm Pacific case **d** same as **b** except for the warm Indian/warm Pacific case

that this enhanced variability of omega applies to greater upward vertical motion variability in the western Pacific, and greater downward vertical motion variability in the Indian sector as the forcing from the Pacific is transmitted to the enhanced downward velocity in the Indian region by the anomalous Walker Circulation. In fact, there is actually a stronger enhancement of variability over parts of the Indian sector (around 70–100°E) in Fig. 9c than for the warm Indian Ocean case in Fig. 9b. Additionally, the uniform SST increase across the Pacific results in greatest nonlinear effects occurring over the western Pacific warm pool west of the Dateline, with small decreases over the cold tongue region to the east.

For both warm Indian Ocean and Pacific Ocean in Fig. 9d, there are increases of vertical velocity variability (positive differences) greater than +2 hPa $s^{-1} \times 10^{-5}$ over both the western Pacific around 150°E as well as over the Indian sector from 60°E to 90°E. Comparing to the changes in mean omega in Fig. 8d, this indicates that the enhanced upward vertical velocity variability in the western Pacific associated with the increased latent heat flux variability (Fig. 7c) and precipitation variability (Fig. 6c) is transmitted via the anomalous Walker

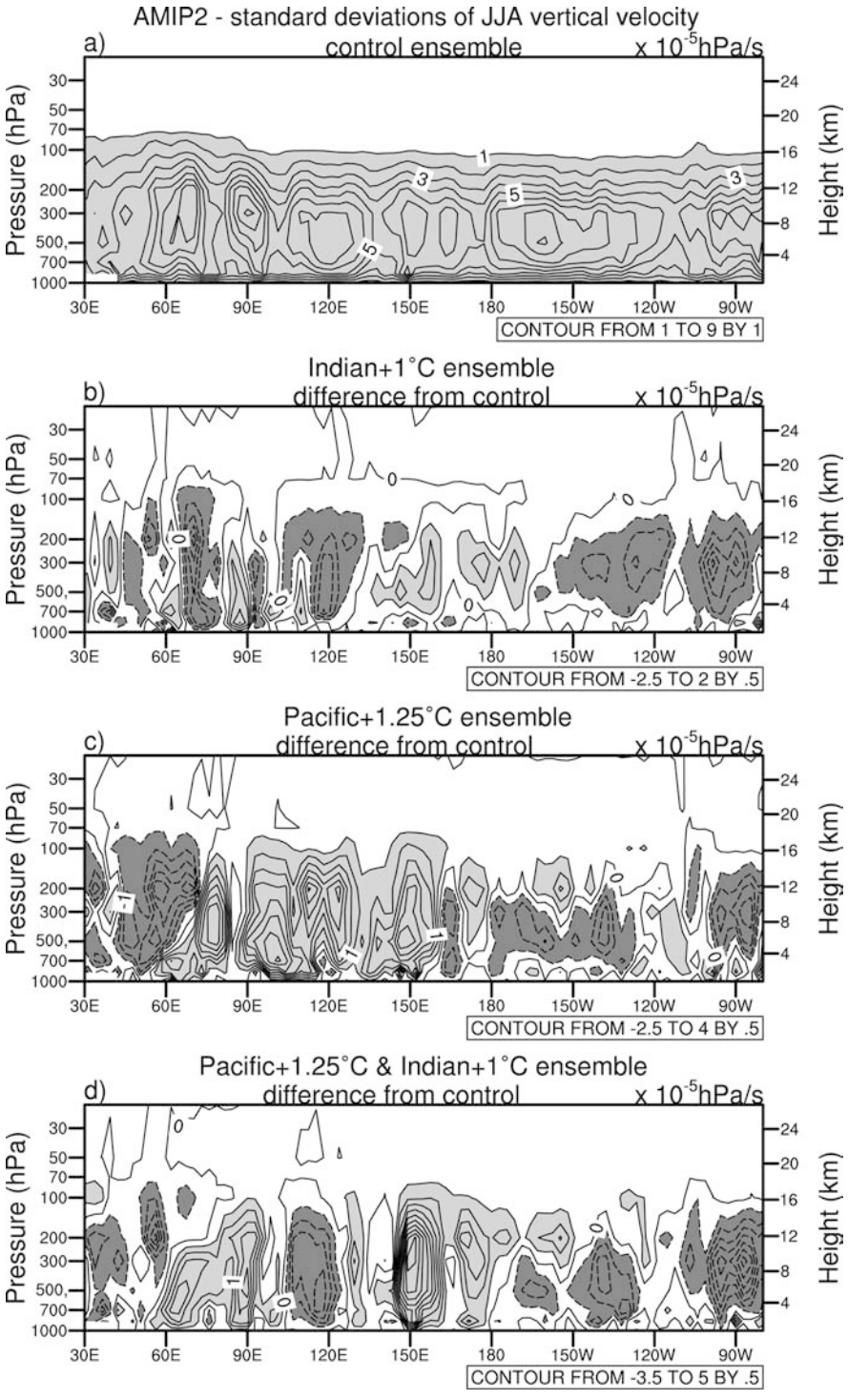

Fig. 9 **a** JJA interannual standard deviation of omega (vertical velocity) for two concatenated control runs with AMIP2 SSTs, 1979–97, specified in the atmospheric model, 10°S to 15°N, contour interval 1 hPa $s^{-1} \times 10^{-5}$, *values* greater than 1 hPa $s^{-1} \times 10^{-5}$ z*shaded*; **b** three member ensemble concatenated interannual standard deviation for the warm Indian Ocean SST experiment minus interannual standard deviation of omega from the control, JJA, contour interval 0.5 hPa $s^{-1} \times 10^{-5}$, *negative areas* (decreased vertical velocity variability) exceeding –0.5 hPa $s^{-1} \times 10^{-5}$ are *dark shaded*, *positive areas* (increased vertical velocity variability) greater than +0.5 hPa $s^{-1} \times 10^{-5}$ are *light shaded*, **c** same as **b** except for the warm Pacific case **d** same as **b** except for the warm Indian/warm Pacific case

Circulation to the Indian monsoon region, thus contributing to enhancing monsoon precipitation variability.

4.5 Coupled model processes

To confirm that the coupled model has similar processes taking place, interannual standard deviations of latent heat flux from the PCM are shown in Fig. 10. For the control in Fig. 10a (comparing to the AMIP2-type experiments in Fig. 7a), values from the coupled model are generally smaller in many areas except for the Pacific ITCZ (PCM values of over 30 W m^{-2} compared to AMIP2 of 20 W m^{-2}) and over India itself where PCM has more than double the interannual standard deviations of latent heat flux compared to the AMIP2-type runs. The oceanic differences between

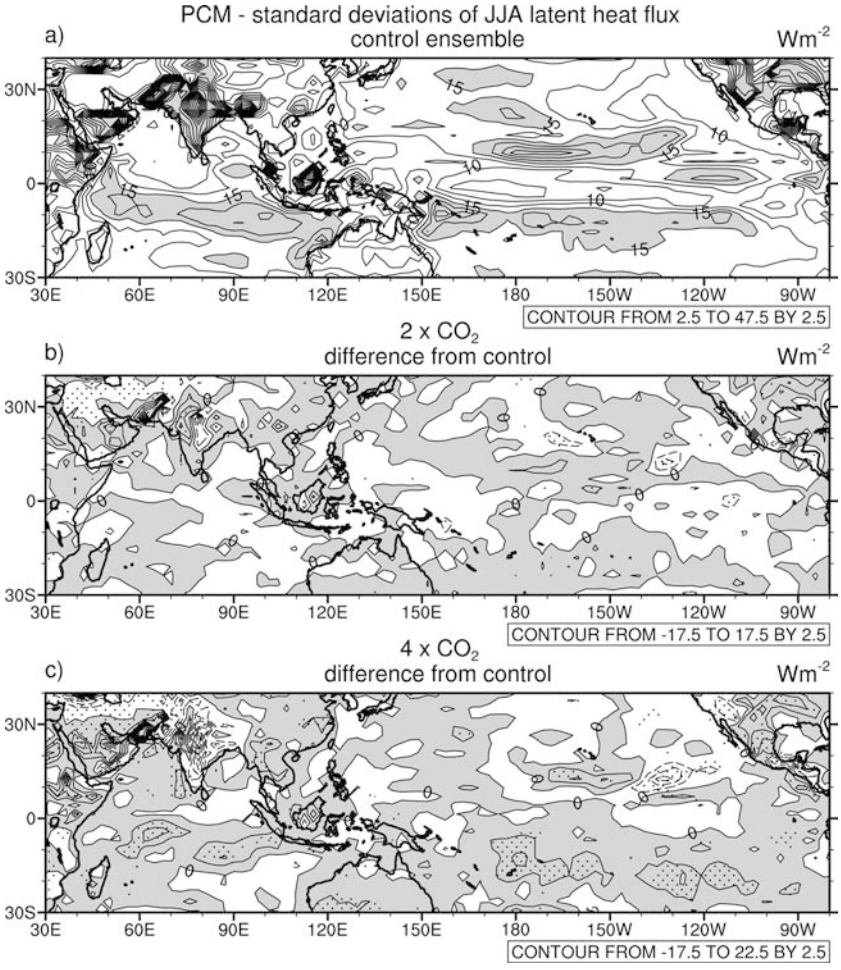

Fig. 10 **a** JJA interannual latent heat flux standard deviations calculated for 300 year period in the PCM (coupled model) control run, contour interval 2.5 W m^2, *values* greater than 15 W m^2*shaded*; **b** interannual latent heat flux standard deviations for 100 year period in stabilized 2 × CO_2 PCM experiment minus control latent heat flux interannual standard deviations, JJA, contour interval 2.5 W m^2, *positive areas shaded*, *stippling* indicates areas exceeding 10% significance level from an *f* test on the ratio of the variances; **c** same as **b** except for 4 × CO_2

latent heat flux variability in the coupled (PCM) and un-coupled (AMIP2-type) models can mostly be traced to systematic errors in the atmosphere and associated coupled model SSTs. For example, the PCM has the Pacific ITCZ positioned nearly 5° of latitude farther north than in the AMIP2-type experiment (comparing Figs. 2a and 5a). Over India, the coupled model systematic error described earlier involves the marginal precipitation zone lying over much of India in the coupled model (Fig. 2a) compared to farther west in the un-coupled model (Fig. 5a). This contributes to greater interannual variability of precipitation (comparing Figs. 3a and 6a) and latent heat flux (Figs. 7a and 10a) over India in the coupled model compared to the uncoupled model.

Regarding differences of latent heat flux variability with increased CO_2 in the coupled model (Fig. 10b, c) compared to the analogous combined effects of warm Indian Ocean and Pacific Ocean SSTs in the uncoupled AMIP2-type experiments in Fig. 7d, there is a similar enhancement of latent heat flux variability in the Pacific ITCZ and SPCZ regions in the coupled model with significant interannual standard deviation differences exceeding 5 W m^{-2} in Fig. 10c, as well as some increases over most of the tropical Indian Ocean. The latent heat flux standard deviation difference patterns from the coupled model are similar for doubling and quadrupling CO_2 in Fig. 10b, c, respectively, with the differences about a factor of three greater in Fig. 10c for a quadrupling of CO_2 compared to a doubling of CO_2 in Fig. 10b. The nonlinear increase of latent heat flux variability associated with a given SST increase is consistent with the mechanism in Fig. 1. These nonlinear effects associated with the Clausius-Clapyron relationship also are relevant to understanding some of the nonlinear local increases of precipitation between 2 × CO_2 and 4 × CO_2 noted in Fig. 2.

To compare the changes in the large-scale east-west circulation in the PCM to those from the uncoupled AMIP2-type sensitivity experiments, Fig. 11 shows mean JJA values of omega for the PCM control run (Fig. 11a), the 2 × CO_2 minus control (Fig. 11b), and 4 × CO_2 minus control (Fig. 11c). Comparing Fig. 11 to the AMIP2-type experiments in Fig. 8, there is a comparable pattern in the control run of the atmosphere-only version (Fig. 8a) and the coupled model (Fig. 11a) with strong vertical velocities (negative values in excess of –20 hPa $s^{-1} \times 10^{-5}$ extending from east of the dateline to near 70°E. Differences in amplitude of omega can be traced directly to the magnitudes of the precipitation in the control runs in Figs. 2a (PCM) and 5a (uncoupled). For example, as noted earlier, the uncoupled AMIP2-

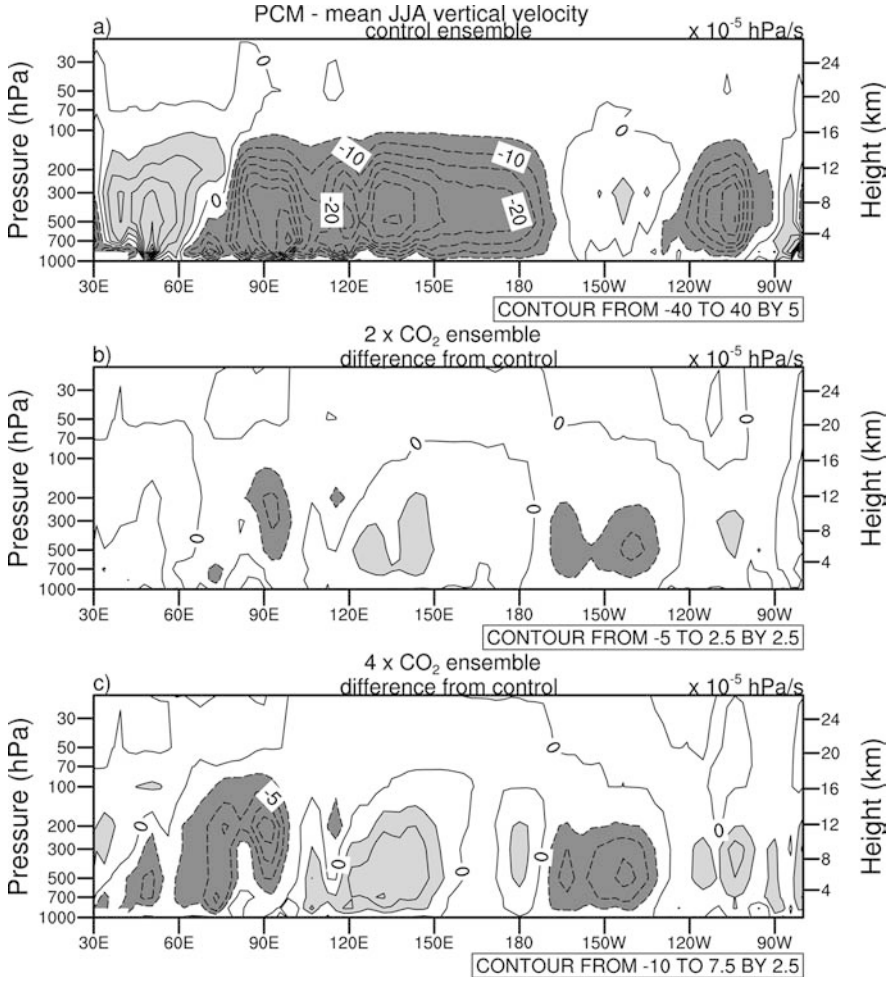

Fig. 11 **a** JJA mean omega (vertical velocity) averaged over 300 years in the PCM (coupled model) control run, 10°S to 15°N, contour interval 5 hPa $s^{-1} \times 10^{-5}$, *values* greater than 5 hPa $s^{-1} \times 10^{-5}$*shaded*; **b** difference of JJA omega for 100 year period in stabilized $2 \times CO_2$ PCM experiment minus control omega, contour interval 2.5 hPa $s^{-1} \times 10^{-5}$, *dashed negative values* (enhanced upward vertical velocity) exceeding –2.5 hPa $s^{-1} \times 10^{-5}$ are *dark shaded*, *positive areas* (enhanced downward vertical velocity) greater than +2.5 hPa $s^{-1} \times 10^{-5}$ are *light shaded*; **c** same as **b** except for $4 \times CO_2$

type control run has greater precipitation maxima farther west in the Indian Ocean in Fig. 5a compared to the PCM coupled model in Fig. 2a. Consequently, the AMIP2-type control run values of omega have negative values over –30 hPa $s^{-1} \times 10^{-5}$ near 65°E, while the PCM has near zero omega at the longitude.

For comparable changes to omega, Fig. 8d from the warm Indian/warm Pacific Ocean AMIP2-type experiments can be compared to Fig. 11b, c for a doubling and quadrupling of CO_2 in the coupled model. For the latter, both show negative differences (enhanced upward vertical velocity) in the Indian and Pacific sectors greater than –2.5 hPa $s^{-1} \times 10^{-5}$ associated with the increased precipitation in those regions in Fig. 2. Omega differences in Fig. 11 greater in magnitude than about 2 hPa $s^{-1} \times 10^{-5}$ are significant at the 10% level (not shown). The pattern in Fig. 11b, c is similar to that simulated in Fig. 8d for the warm Indian/warm Pacific Ocean AMIP2-type experiments where there is enhanced upward vertical motion around 90°E in the Indian monsoon region, as well as near 150°E to 120°W in the Pacific. There is also greater subsidence (positive omega differences) over the southeast Asian region from about 110°E to 150°E in the warm Indian/warm Pacific Ocean AMIP2-type experiments (Fig. 8d) and the coupled model increased CO_2 experiments (Fig. 11b, c). Most of the increases in magnitude of the omega differences between doubling and quadrupling of CO_2 are greater than a factor of two, consistent with the non-linear precipitation changes (Fig. 2b, c). West of about 60°E there is anomalous upward vertical motion in Fig. 11c compared to opposite sign anomalies in Fig. 8d. With the large increase of CO_2 in Fig. 11c, the African land areas warm considerably, thus driving anomalous upward vertical motion. In Fig. 8d, only the Indian Ocean is warmer and this, in contrast to Fig. 11c, drives anomalous subsidence to the west over Africa.

It was concluded from the AMIP2-type experiments that the specified increases in SST in the tropical Indian Ocean and Pacific Ocean had a non-linear effect on increasing evaporation and thus latent heat flux variability, which then had a comparable effect in increasing precipitation variability that was reflected in increased variability of omega. These changes were communicated by the large-scale east-west circulation in the atmosphere, with the Pacific proving to be dominant due to the warmer base state SSTs there compared to the Indian Ocean. For the coupled model, all of these changes for an increase in CO_2 are consistent with the uncoupled

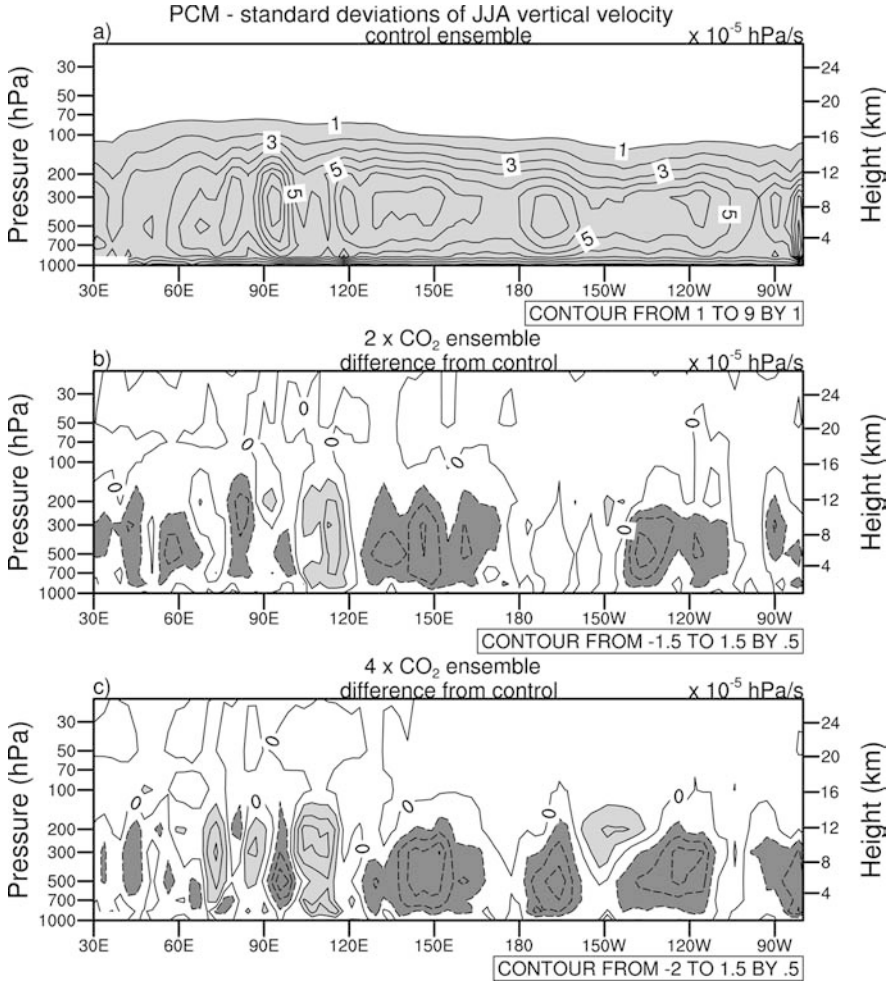

Fig. 12 **a** interannual standard deviations of JJA omega (vertical velocity) for 300 year period in the PCM (coupled model) control run, 10°S to 15°N, contour interval 1 hPa $s^{-1} \times 10^{-5}$, *values* greater than 1 hPa $s^{-1} \times 10^{-5}$ *shaded*; **b** difference of JJA omega interannual standard deviations for 100 year period in stabilized $2 \times CO_2$ PCM experiment minus interannual standard deviations of control omega, contour interval 0.5 hPa $s^{-1} \times 10^{-5}$, *dashed negative values* (decreased vertical velocity variability) exceeding –0.5 hPa $s^{-1} \times 10^{-5}$ are *dark shaded*, *positive areas* (enhanced vertical velocity variability) greater than +0.5 hPa $s^{-1} \times 10^{-5}$ are *light shaded*; **c** same as **b** except for $4 \times CO_2$

AMIP2-type experiments. This comparison is shown in Fig. 12 for changes in standard deviation of omega for the coupled model for a doubling and quadrupling of CO_2. Similar to the warm Indian/warm Pacific Ocean sensitivity experiment in Fig. 9d, there are increases in omega variability in the Indian sector in the same areas where there were the largest increases in vertical velocity in Fig. 11b, c, from about 65 to 120°E, and in the Pacific sector around 150°W. The increases of omega variability are greater for a quadrupling of CO_2 (maxima in the Indian and Pacific sectors greater than 1.5 hPa $s^{-1} \times 10^{-5}$) in Fig. 12c than for doubling in Fig. 12b (maxima in those regions of around 1 hPa $s^{-1} \times 10^{-5}$), consistent with changes discussed in relation to precipitation and latent heat flux.

5 Conclusions

A global coupled model with stabilized $2 \times CO_2$ and $4 \times CO_2$ shows increases in both mean and interannual variability of Indian monsoon rainfall in agreement with increased CO_2 results from other coupled models. To examine the mechanisms for these changes in the coupled model, a set of uncoupled AMIP2-type sensitivity experiments are run with warmer Indian Ocean, warmer Pacific Ocean, and combined warmer Indian and Pacific Ocean SSTs. We hypothesize that the nonlinear effects associated with the Clausius-Clapeyron relationship between SST and evaporation should produce enhancements to mean evaporation and thus latent heat flux (to contribute to an enhanced moisture source for increased mean monsoon precipitation), as well as greater variability of evaporation and latent heat flux (to contribute to greater variability of monsoon precipitation). The source of these effects could arise from either Indian or Pacific Ocean SST warming, with effects being transmitted by the large-scale east-west atmospheric circulation.

Results from the sensitivity experiments confirm the hypothesis regarding the changes to monsoon precipitation variability, and show that the remote effects from the Pacific are a primary cause for enhanced monsoon precipitation variability as opposed to regional effects from the Indian Ocean. The warmer Indian Ocean is the main contributor to the increase of Indian monsoon seasonal mean precipitation, with the influence from the tropical Pacific tending to reduce the monsoon precipitation increases.

The mechanism for these changes in the CO_2 climate change experiments begins with Clausius/Clapeyron-related changes in moisture source. With the increase of CO_2 and warmer base state SSTs, there is greater evaporation (and thus latent heat flux) contributing to an increased moisture source for greater mean monsoon precipitation. Enhanced variability of evaporation and latent heat flux contribute to increased Indian monsoon variability. This occurs in the coupled model even though the SST variability in the tropical Pacific does not change significantly with increased CO_2 (Washington et al. 2000). Similarly in the AMIP2-type sensitivity experiments, the specified SST variability does not change, yet the interannual variability of monsoon precipitation increases mainly due to forcing from the tropical western Pacific.

The regions where these changes occur are important for their influences on mean and interannual variability of Indian monsoon rainfall. Increased moisture source from the warmer Indian Ocean with increased CO_2, as confirmed by the sensitivity experiments, contributes most to greater mean monsoon precipitation. However, enhanced evaporation and latent heat flux variability is more important in the tropical Pacific for contributing to increased monsoon variability. The greater latent heat flux variability is manifested by increased precipitation variability in the tropical Pacific which is then transmitted by the large-scale east-west circulation in the atmosphere to the Indian sector as indicated by changes in vertical velocity (omega). The result is enhanced monsoon precipitation variability. Similar changes in latent heat flux variability are occurring in the Indian Ocean as well, but those changes have mainly local effects. The main contributor to greater monsoon variability simulated in the warmer climate comes from the Pacific in these experiments. It is also likely that related nonlinear changes in convective available potential energy (CAPE) are contributing to the variability changes. This is being explored in a subsequent study.

These results have implications that extend beyond the present set of experiments. For example, decadal-time scale variability in the Pacific (i.e., tropical Pacific SSTs warming and cooling at decadal time scales) could affect interannual variability of monsoon precipitation. If tropical Pacific SSTs were anomalously warm for 10–20 years, then, even without any change in El Nino amplitude, the interannual variability of monsoon precipitation could increase through the mechanisms described in the present study.

Acknowledgements A portion of this study was supported by the Office of Biological and Environmental Research, US Department of Energy, as part of its Climate Change Prediction Program. The National Center for Atmospheric Research is sponsored by the National Science Foundation.

References

Bonan GB (1998) The land surface climatology of the NCAR land surface model (LSM 1.0) coupled to the NCAR Community Climate Model (CCM3). J Clim 11: 1307–1326

Chandrasekar A, Kitoh A (1998) Impact of localized sea surface temperature anomalies over the equatorial Indian Ocean on the Indian summer monsoon. J Meteorol Soc Japan 76: 841–853

Cubasch U, Meehl GA, Boer GJ, Stouffer RJ, Dix M, Noda A, Senior CA, Raper S, Yap KS (2001) Projections of future climate change. In: Houghton JT, Ding Y, Griggs DJ, Noguer M, van der Linden P, Dai X, Maskell K, Johnson CI (eds) Climate change 2001: The scientific basis. Contribution of Working Group I to the Third Assessment Report of the Intergovernmental Panel on Climate Change. Cambridge University Press, Cambridge, UK, pp 525–582

Douville H, Royer JF, Polcher J, Cox P, Gedney N, Stephenson DB, Valdes PJ (2000) Impact of CO_2 doubling on the Asian summer monsoon: robust versus model-dependent responses. J Meteorol Soc Japan 78: 421–439

Hu ZZ, Latif M, Roeckner E, Bengtsson L (2000) Intensified Asian summer monsoon and its variability in a coupled model forced by increasing greenhouse gas concentrations. Geophys Res Lett 27: 2681–2684

Ju J, Slingo J (1995) The Asian summer monsoon and ENSO. Q J R Meteorol Soc 121: 1133–1168

Kiehl JT, Hack JJ, Bonan G, Boville B, Williamson D, Rasch P (1998) The National Center for Atmospheric Research Community Climate Model (CCM3). J Clim 11: 1131–1149

Kitoh A, Yukimoto S, Noda A, Motoi T (1997) Simulated changes in the Asian summer monsoon at times of increased atmospheric CO_2. J Meteorol Soc Japan 75: 1019–1031

Lal M, Meehl GA, Arblaster JM (2000) Simulation of Indian summer monsoon rainfall and its intraseasonal variability. Regional Environ Change 1: 163–179

Lal M, Nozawa T, Emori S, Harasawa H, Takahashi K, Kimoto M, Abe-Ouchi A, Nakajima T, Takemura T, Numaguti A (2001) Future climate change: Implications for Indian summer monsoon and its variability. Current Sci 81(9): 1196–1207

Lau NC, Nath MJ (2000) Impact of ENSO on the variability of the Asian-Australian monsoon as simulated in GCM experiments. J Clim 13: 4287–4309

May W (2002) Simulated changes of the Indian summer monsoon under enhanced greenhouse gas conditions in a global time-slice experiment. Geophys Res Lett 29(7): 10.1029/2001GL013808

Meehl GA (1987) The annual cycle and interannual variability in the tropical Pacific and Indian Ocean regions. Mon Weather Rev 115: 27–50

Meehl GA, Arblaster JM (1998) The Asian-Australian monsoon and El Nino-Southern Oscillation in the NCAR Climate System Model. J Clim 11: 1357–1387

Meehl GA, Arblaster JM (2002) GCM sensitivity experiments for the Indian monsoon and tropospheric biennial oscillation transition conditions. J Clim 15: 923–944

Meehl GA, Washington WM (1993) South Asian summer monsoon variability in a model with doubled atmospheric carbon dioxide concentration. Science 260: 1101–1104

Meehl GA, Gent P, Arblaster JM, Otto-Bliesner B, Brady E, Craig A (2001) Factors that affect amplitude of El Nino in global coupled climate models. Clim Dyn 17: 515–526

Parthasarathy B, Rupa Kumar K, Munot AA (1991) Evidence of secular variations in Indian monsoon rainfall-circulation relationships. J Clim 4: 927–938

Rasmusson EM, Carpenter TH (1983) The relationship between eastern equatorial Pacific sea surface temperatures and rainfall over India and Sri Lanka. Mon Weather Rev 111: 517–528

Slingo JM, Annamalai H (2000) 1997: The El Nino of the century and the response of the Indian summer monsoon. Mon Weather Rev 128: 1778–1797

Timmermann A, Oberhuber J, Bacher A, Esch M, Latif M, Roeckner E (1999) Increased El Nino frequency in a climate model forced by future greenhouse warming. Nature 398: 694–697

Washington WM, Weatherly JW, Meehl GA, Semtner Jr. AJ, Bettge TW, Craig AP, Strand Jr. WG, Arblaster JM, Wayland VB, James R, Zhang Y (2000) Parallel climate model (PCM) control and transient simulations. Clim Dyn 16: 755–774

Webster PJ, Yang S (1992) Monsoon and ENSO: Selectively interactive systems. Q J R Meteorol Soc 118: 877–926

Xie P, Arkin PA (1996) Analyses of global monthly precipitation using gauge observations, satellite estimates, and numerical model predictions. J Clim 9: 840–858